Generalization of the atomic random-phase-approximation method for diatomic molecules: N_2 photoionization cross-section calculations

S. K. Semenov,[1] N. A. Cherepkov,[1] G. H. Fecher,[2] and G. Schönhense[2]
[1]*State University of Aerospace Instrumentation, 190000 St. Petersburg, Russia*
[2]*Institut für Physik, Johannes-Gutenberg-Universität, 55099 Mainz, Germany*
(Received 1 June 1999; published 10 February 2000)

Partial and total photoionization cross sections of N_2 molecule are calculated using the generalization of the random-phase approximation (RPA) which earlier has been successfully applied to the description of the atomic photoionization processes. According to this method, at first the Hartree-Fock (HF) ground-state wave functions are calculated in prolate spheroidal coordinates using the fixed-nuclei approximation. With their help the zero order basis set of single particle Hartree-Fock wave functions containing both discrete excited states and continuous spectrum is calculated in the field of a frozen core of a singly charged ion. The calculations are performed for all four valence shells of N_2 molecule, $3\sigma_g$, $1\pi_u$, $2\sigma_u$, and $2\sigma_g$, with the intershell correlations fully taken into account within the RPA method. It is demonstrated that different intershell correlations, especially between three outer shells, play an important role in photoionization process. Examples of the influence of intershell correlations on several transitions are presented. Partial and total photoionization cross sections of N_2 molecule obtained by this method in the photon energy range from ionization threshold up to 70 eV are in a good agreement with the existing experimental data and with the recent RPA calculations [Cacelli *et al.*, Phys. Rev. A **57**, 1895 (1998)].

PACS number(s): 33.80.Eh

I. INTRODUCTION

Molecular nitrogen is one of the best studied diatomic molecules due to its importance as a main constituent of the atmosphere, and due to its relative simplicity for both experimental and theoretical investigations. A rather complete list of references on different photoionization studies of the N_2 molecule can be found in several recent publications devoted to the comparison of theoretical photoionization cross-section calculations with the experimental data [1–7]. These calculations were performed in the random phase approximation (RPA) which earlier has been very successfully applied to the description of the atomic photoionization processes [8,9]. One of advantages of the RPA method is that the photoionization cross sections calculated in the length and velocity forms coincide, while in the Hartree-Fock (HF) approximation they can differ substantially, sometimes by a factor of 2. The goal of this work is to generalize the RPA method as it was developed in [8], for diatomic molecules, and to check its efficiency in molecular photoionization cross-section calculations. As a first demonstration of this method we calculated the photoionization cross section of H_2 molecule [10] which has been studied previously in a number of papers. Our theory is in a remarkably good agreement with the recent experimental data. The first results of the analogous calculations for N_2 molecule are presented here.

There were already several studies of N_2 molecule using different versions of RPA, all of them being different from the version described here. In particular, Cacelli *et al.* [1] used a large L^2 basis sets of one center Gaussian-type orbitals for a description of a short-range behavior of continuous spectrum wave functions, and a *K*-matrix based technique in their RPA calculations. Shirmer and Mertins [2] restricted their consideration of RPA by taking into account only the first order of perturbation theory, and therefore their cross sections in the length and velocity forms do not coincide. Veseth [3] and Yabushita *et al.* [5] used the RPA method based on an analytic continuation of polarizability calculated for complex values of the frequency, avoiding in this way calculations of continuous spectrum wave functions, the main problem in applying the RPA for diatomic molecules. Lucchese and Zurales [4] implemented the RPA method in the form of closed-coupled equations which were solved using the Schwinger variational method with Padé-approximant corrections. In [6,7] the time-dependent Hartree-Fock approximation, which is equivalent to the RPA, was used in combination with the so-called Stieltjes-Chebyshev moment theory. These different versions of RPA gave rather different results for the photoionization cross section of N_2 molecule.

We calculated the partial and total photoionization cross sections of all four valence shells, $3\sigma_g$, $1\pi_u$, $2\sigma_u$, and $2\sigma_g$, of N_2 molecule with the intershell correlations fully taken into account within the RPA method. We checked that the correlations with the $1\sigma_u$, and $1\sigma_g$ shells are not important at the photon energies considered by us. Earlier the correlations between all four shells have been taken into account only in [1,4,5,7], but in [5,7] the consideration have been restricted by the $^1\Sigma_u^+$ final states, that is by the transitions with $\Delta m = 0$ where m is the projection of orbital angular momentum of electron, and in [4] the calculations have been restricted by a narrower photon energy region. Only in [1] the calculations have been performed on the same level of sophistication as here, and in the same photon energy range, therefore in the following we shall compare our RPA cross sections mainly with the results of this paper. Correlations between three valence shells, $3\sigma_g$, $1\pi_u$, and $2\sigma_u$, have been taken into account in [3,6].

In accord with [8], our RPA calculations proceed as following. At first the HF ground state wave functions are cal-

culated in the fixed-nuclei approximation. With their help the zero order basis set of single particle HF wave functions of discrete excited states and of the continuous spectrum is calculated in the field of a frozen core of a singly charged ion (the one particle–one hole excited states). With this basis the dipole and the Coulomb matrix elements are calculated. As the next step we are looking for the dipole matrix elements in RPA by solving the corresponding RPA equation, without calculating explicitly the wave functions in RPA. In the integral RPA equation for the dipole matrix elements the infinite integration over the continuous spectrum is substituted approximately by a finite summation, and in that way the integral equation is transformed into a set of algebraic equations which is solved by matrix inversion. The dipole matrix elements obtained as a solution of the RPA equation can be used for calculations of photoionization cross section, angular distribution and spin polarization of photoelectrons. In this paper we report only on the partial cross-section calculations, the angular distributions will be discussed elsewhere. Also we do not discuss the autoionization structures corresponding to one-particle excitations which can be described within the RPA method.

It should be noted that solving the RPA equations themselves for molecules is quite similar to that for atoms. The main problem in realization of the RPA method in molecules consists in calculation of one-electron Hartree-Fock continuous spectrum wave functions forming, together with the discrete excited states, the orthonormal basis set of HF wave functions. For the success of the RPA calculations it is crucially important to use the exact HF wave functions without any simplification like localization of the exchange interaction, and so on. Therefore we paid a special attention to the quality of our HF wave functions. It is becoming usual now to calculate the bound state wave functions of diatomic molecules using a partial wave expansion in prolate spheroidal coordinates [11–13]. As compared to usual expansion in spherical coordinates, this method substantially reduces the number of terms necessary to take into account in order to reach high accuracy in calculations. That is because the prolate spheroidal coordinates are more natural in diatomic molecules and provide separation of coordinates for one-electron problem. Therefore we use this method for continuous spectrum wave function calculations, too. It does not give any additional difficulties and allows to perform calculations more efficiently. As to the deep atomiclike bound states in molecules, they are also calculated accurately by this method. This was demonstrated earlier in [14] by calculating the Ne atom wave functions in prolate spheroidal coordinates with the nuclear charges $Z_1=10$, $Z_2=0$, and the ''internuclear'' distance equal to $1.5a_0$.

II. THEORY

A. General relations

Keeping in mind the further applications for calculations of the angular distributions of photoelectrons, it is convenient to determine photoionization parameters through the photoelectron orbital $\psi_{\boldsymbol{k}}^{(-)}(\boldsymbol{r})$ with the incoming-wave boundary condition. Here $\boldsymbol{k}$ is the electron momentum and $\boldsymbol{r}$ is its coordinate. The partial wave expansion of this orbital in the molecular frame is given as usual by [15–17]

$$\psi_{\boldsymbol{k}}^{(-)}(\boldsymbol{r})=\sum_{l,m} f_{\varepsilon lm}(\boldsymbol{r})Y_{lm}^{*}(\hat{\boldsymbol{k}}), \tag{1}$$

where

$$f_{\varepsilon lm}(\boldsymbol{r})|_{r\to\infty}\sim\left(\frac{2}{\pi k}\right)^{1/2}\frac{1}{2ir}\left(Y_{lm}(\hat{\boldsymbol{r}})e^{i\vartheta(r)}-\sum_{l'} Y_{l'm}(\hat{\boldsymbol{r}})S_{ll'm}^{*}e^{-i\vartheta(r)}\right), \tag{2}$$

$\vartheta(r)=kr+k^{-1}\ln 2kr$, and the function (2) is normalized to an energy δ function. Then the differential photoionization cross section in the length (L) and velocity (V) forms can be written as (atomic units $\hbar=m=e=1$ are used in this paper)

$$d\sigma^{L,V}(\omega)/d\Omega_{\mathbf{k}}=4\pi^2 a a_0^2\omega\sum_{\mu}|e_{\mu}\langle\psi^{(-)}(\boldsymbol{k},\boldsymbol{r})|d_{\mu}^{L,V}|i\rangle|^2, \tag{3}$$

where ω is the photon energy, $\Omega_{\mathbf{k}}$ denotes the spherical angles of the vector $\boldsymbol{k}$, α is the fine-structure constant, a_0 is the Bohr radius, $|i\rangle$ means the initial state of the molecule, and e_{μ} are the spherical projections of the photon polarization vector,

$$d_{\mu}^{L}=\sqrt{\frac{4\pi}{3}}rY_{1\mu}(\hat{\boldsymbol{r}}),$$

$$d_{\mu}^{V}=\begin{cases}\dfrac{1}{\sqrt{2}}\left(\mp\dfrac{\partial}{\partial x}\pm i\dfrac{\partial}{\partial y}\right) & \text{for } \mu=\pm 1\\ \dfrac{\partial}{\partial z} & \text{for } \mu=0.\end{cases} \tag{4}$$

Since the spherical functions $Y_{lm}(\hat{\boldsymbol{k}})$ form an orthonormal set, the total photoionization cross section can be obtained from Eq. (3) by integrating over the photoelectron ejection angle and averaging over all polarizations

$$\sigma^{L,V}(\omega)=\frac{4}{3}\pi^2 a a_0^2\omega\sum_{\mu}\sum_{l,m}|\langle f_{\varepsilon lm}(\boldsymbol{r})|d_{\mu}^{L,V}|i\rangle|^2. \tag{5}$$

Only the electronic degrees of freedom are considered here within the Born-Oppenheimer approximation.

Instead of the functions $f_{\varepsilon lm}(\boldsymbol{r})$ which include an imaginary part, we prefer to calculate the set of other functions $\varphi_{\varepsilon lm}(\boldsymbol{r})$ which are real and which are the linear combinations of the functions $f_{\varepsilon lm}(\boldsymbol{r})$. We shall do it following the ideas of the K-matrix method [15,17], and a method of phases [18]. In the latter paper it was proposed to expand the functions $\psi^{(-)}(\mathbf{r})$ not in spherical harmonics as it is usually done, but in some other complete basis set which is energy dependent, that is for each photoelectron energy there is a new set of basis wave functions. As it was noticed in [15,19], the sets of wave functions corresponding to different types of boundary conditions are interrelated by unitary transformations, and

we shall use this fact. Our method consists in the following. For a given photoelectron energy ε and momentum $k(\varepsilon = k^2/2)$ we are looking for a solution satisfying the asymptotic condition

$$\varphi_{\varepsilon lm}(\boldsymbol{r})|_{r\to\infty} \sim \frac{1}{r}\left(\frac{2}{\pi k}\right)^{1/2} \sum_{l'} c_{ll'}^{\varepsilon m} Y_{l'm}(\hat{\boldsymbol{r}}) \sin(\vartheta(r) + \delta_{ll'}^{\varepsilon m}),$$

$$\sum_{l'} (c_{ll'}^{\varepsilon m})^2 = 1, \tag{6}$$

or in another form

$$\varphi_{\varepsilon lm}(\boldsymbol{r})|_{r\to\infty} \sim \left(\frac{2}{\pi k}\right)^{1/2} \frac{1}{2ir} \sum_{l'} c_{ll'}^{\varepsilon m} Y_{l'm}(\Omega_r) \times e^{i\delta_{ll'}^{\varepsilon m}} (e^{i\vartheta(r)} - e^{-i\vartheta(r)} e^{-2i\delta_{ll'}^{\varepsilon m}}) \tag{6a}$$

and the orthonormalization conditions

$$\langle \varphi_{\varepsilon lm} | \varphi_{\varepsilon' l'm'} \rangle = \delta_{ll'} \delta_{mm'} \delta(\varepsilon - \varepsilon'). \tag{6b}$$

We do not fix at this moment the boundary conditions of the wave function since we are going to get the generalized relations for the $\psi^{(-)}$ function which are valid for any boundary condition including those used in [17,18]. In the case of separable coordinates considered in [18] the phases in Eq. (6) are independent of the index l', and the coefficients $c_{ll'}^{\varepsilon m} = c_l^{\varepsilon m} \delta_{ll'}$ are found as solutions of the equations for determination of a separation constant. Since in our case the coordinates are not separable, the phases in general depend on l', and we could not use the condition of separability for determining the set of solutions. Instead of that, we are using the following procedure. We introduce a new set of functions

$$\Phi_{lm}^{\varepsilon}(\hat{\boldsymbol{k}}) = \sum_{l'} c_{ll'}^{\varepsilon m} Y_{l'm}(\Omega_{\mathbf{k}}) \exp(i\delta_{ll'}^{\varepsilon m}), \tag{7}$$

which for any ε form a complete orthonormal set on the unit sphere, that is

$$\int \Phi_{lm}^{\varepsilon}(\hat{\boldsymbol{k}}) \Phi_{l_1 m_1}^{\varepsilon *}(\hat{\boldsymbol{k}}) d\Omega_{\boldsymbol{k}} = \delta_{ll_1} \delta_{mm_1}, \tag{8}$$

$$\sum_{l,m} \Phi_{lm}^{\varepsilon}(\hat{\boldsymbol{k}}) \Phi_{lm}^{\varepsilon *}(\hat{\boldsymbol{k}}') = \delta(\hat{\boldsymbol{k}} - \hat{\boldsymbol{k}}'). \tag{9}$$

Inserting Eq. (7) into Eqs. (8) and (9), and using the fact that the spherical functions form the complete orthonormal set on the unit sphere, we obtain the following conditions for the parameters $c_{ll'}^{\varepsilon m}$:

$$\int \sum_{l'} c_{ll'}^{\varepsilon m} Y_{l'm}(\Omega_{\mathbf{k}}) \exp(i\delta_{ll'}^{\varepsilon m}) \sum_{l''} c_{l_1 l''}^{\varepsilon m_1} Y_{l''m_1}^{*}(\Omega_{\mathbf{k}}) \exp(-i\delta_{l_1 l''}^{\varepsilon m_1}) d\Omega_{\mathbf{k}} = \sum_{l'} c_{ll'}^{\varepsilon m} c_{l_1 l'}^{\varepsilon m} \exp[i(\delta_{ll'}^{\varepsilon m} - \delta_{l_1 l'}^{\varepsilon m})] = \delta_{ll_1}, \tag{10}$$

$$\sum_{l} c_{ll'}^{\varepsilon m} c_{ll''}^{\varepsilon m} \exp[i(\delta_{ll'}^{\varepsilon m} - i\delta_{ll''}^{\varepsilon m})] = \delta_{l'l''}. \tag{11}$$

After that we can present the function $\psi_k^{(-)}(\boldsymbol{r})$ as an expansion in these functions in the same way as it was done in Eq. (1) with the partial wave expansion,

$$\psi_{\boldsymbol{k}}^{(-)}(\boldsymbol{r}) = \sum_{l,m} \varphi_{\varepsilon lm}(\boldsymbol{r}) \Phi_{lm}^{\varepsilon *}(\hat{\boldsymbol{k}}). \tag{12}$$

The functions $\varphi_{\varepsilon lm}(\boldsymbol{r})$ having the asymptotic behavior (6) are connected with the functions $f_{\varepsilon lm}(\boldsymbol{r})$ defined in Eqs. (1) and (2) by the relation

$$\varphi_{\varepsilon lm}(\boldsymbol{r}) = \sum_{l'} c_{ll'}^{\varepsilon m} f_{\varepsilon l'm}(\boldsymbol{r}) \exp(i\delta_{ll'}^{\varepsilon m}), \tag{13}$$

or, since $c_{ll'}^{\varepsilon m} \exp(i\delta_{ll'}^{\varepsilon m})$ form a unitary matrix,

$$f_{\varepsilon lm}(\boldsymbol{r}) = \sum_{l'} c_{l'l}^{\varepsilon m} \varphi_{\varepsilon l'm}(\boldsymbol{r}) \exp(-i\delta_{l'l}^{\varepsilon m}). \tag{14}$$

To verify the equivalence of the expansions (1) and (12), let us insert Eqs. (13) and (7) into Eq. (12) and use the conditions (10) and (11)

$$\begin{aligned} \psi_{\mathbf{k}}^{(-)}(\boldsymbol{r}) &= \sum_{l,m} \varphi_{\varepsilon lm}(\boldsymbol{r}) \Phi_{lm}^{\varepsilon *}(\hat{\boldsymbol{k}}) \\ &= \sum_{l,m} \sum_{l',l''} f_{\varepsilon l'm}(\boldsymbol{r}) Y_{l''m}^{*}(\Omega_{\mathbf{k}}) c_{ll''}^{\varepsilon m} c_{ll''}^{\varepsilon m} \\ &\quad \times \exp[i(\delta_{ll'}^{\varepsilon m} - i\delta_{ll''}^{\varepsilon m})] \\ &= \sum_{l,m} f_{\varepsilon lm}(\boldsymbol{r}) Y_{lm}^{*}(\Omega_{\mathbf{k}}). \end{aligned} \tag{15}$$

So, the proposed method consists in calculation, instead of the functions $f_{\varepsilon lm}(\boldsymbol{r})$ which include an imaginary part, the other real functions $\varphi_{\varepsilon lm}(\boldsymbol{r})$ which are the linear combinations of the functions $f_{\varepsilon lm}(\boldsymbol{r})$. Since there are simple relations (13) and (14) between these two basis sets, we can easily transform our results into the standard form with the basis set (2) in order to make the comparison with calcula-

tions of other authors or with the values extracted from the experimental data in a complete experiment [20]. Both conditions (8) and relations (13) and (14) which are used for the transformation of our results to the usual expansion in spherical harmonics are simpler than the analogous matrix relations in the *K*-matrix method [17].

B. RPA equation and its solution

Originally the RPA approximation has been introduced for the description of the high density electron gas in solids. Later it was proved [8] that the RPA can be successfully applied for the description of many-electron correlations in atoms, too, provided the inhomogeneity of atoms is taken into account from the very beginning by the use of the HF wave functions as the zero order approximation. Evidently, on the same grounds the RPA method can be successfully applied to molecules as well. We shall use both the HF and the RPA approximations for defining the dipole matrix elements introduced above, and the cross sections. According to [8] the RPA equation for the dipole matrix elements can be written as

$$\langle \varepsilon lm|D_\mu|i\rangle = \langle \varepsilon lm|d_\mu|i\rangle + \sum_{j\leqslant F}\sum_{\varepsilon'>F}\sum_{l',m'}\left[\frac{\langle \varepsilon' l'm'|D_\mu|j\rangle\langle j,\varepsilon lm|U|\varepsilon' l'm',i\rangle}{\omega-\varepsilon'+\varepsilon_j+i\delta} - \frac{\langle j|D_\mu|\varepsilon' l'm'\rangle\langle \varepsilon' l'm',\varepsilon lm|U|j,i\rangle}{\omega+\varepsilon'-\varepsilon_j-i\delta}\right]. \tag{16}$$

Here i,j mean the set of quantum numbers necessary to specify the bound state wave function including the projection of the angular momentum on the molecular axis m_i, m_j, $\langle \varepsilon lm|D_\mu|i\rangle$ and $\langle \varepsilon lm|d_\mu|i\rangle$ mean the dipole matrix elements in the RPA and in the HF approximations, respectively, $\langle j,\varepsilon lm|U|\varepsilon' l'm',i\rangle$ is the Coulomb matrix element defined as

$$\langle j,\varepsilon lm|U|\varepsilon' l'm',i\rangle = \langle j,\varepsilon lm|V|\varepsilon' l'm',i\rangle - \langle j,\varepsilon lm|V|i,\varepsilon' l'm'\rangle, \tag{17}$$

where

$$\langle j,\varepsilon lm|V|\varepsilon' l'm',i\rangle = \int \varphi_i^*(\boldsymbol{r})\varphi_{\varepsilon lm}^*(\boldsymbol{r}')|\boldsymbol{r}-\boldsymbol{r}'|^{-1} \times \varphi_{\varepsilon' l'm'}(\boldsymbol{r})\varphi_i(\boldsymbol{r}')d\boldsymbol{r}d\boldsymbol{r}', \tag{18}$$

the summation over $j\leqslant F$ in Eq. (16) means the summation over all occupied states (that is the states below the Fermi level), the summation over unoccupied states $\varepsilon'>F$ above the Fermi level includes both the summation over the discrete excited states and integration over the continuous spectrum, so that Eq. (16) is an integral equation, and in the denominators $\delta\to+0$. Since there is a pole in the integrand of Eq. (16), the solutions D_μ are the complex values while the HF matrix elements d_μ are real.

One-electron ground state wave functions are the solutions of the self-consistent HF equations

$$\left[-\frac{\nabla^2}{2}-\frac{Z_i}{r_1}-\frac{Z_2}{r_2}+\sum_{j=1}^{n}2J_{jj}(\boldsymbol{r})\right]\varphi_i(\boldsymbol{r})-\sum_{j=1}^{n}J_{ji}(\boldsymbol{r})\varphi_j(\boldsymbol{r}) = \varepsilon_i\varphi_i(\boldsymbol{r}), \tag{19}$$

where

$$J_{ij}(\boldsymbol{r}) = \int \varphi_i^*(\boldsymbol{r}')|\boldsymbol{r}-\boldsymbol{r}'|^{-1}\varphi_j(\boldsymbol{r}')d\boldsymbol{r}' \tag{20}$$

describes the exchange interaction when $i\neq j$ and the direct interaction when $i=j$.

For the application of the many-body theory in general, and of the RPA approximation in particular, we need to define the zero order complete basis set of one-particle wave functions. In the HF approximation we need to use Eq. (19) with fixed wave functions for all occupied states as an equation generating such a complete basis set. With this basis set we must solve the RPA equation (16) for the dipole matrix elements. But if we shall use Eq. (19) for calculating the wave functions of excited states of both discrete and continuous spectrum, we obtain the wave functions $\varphi_{\varepsilon lm}(\boldsymbol{r})$ calculated in the field of a neutral molecule which does not correspond to the physics of the photoionization process. In reality the photoelectron is moving in the field of a singly charged molecular ion. To take it into account, we must exclude one electron from the HF field in which the photoelectron is moving, leaving the one-particle wave functions in the HF potential the same as they have been found for the ground state of the molecule. In other words, we need to calculate the excited state wave functions in the field of a frozen core of a singly charged molecular ion with the hole state in the shell from which the electron has been ejected. Following the procedure described in [8], we can perform a redefinition of the excited state wave functions in order to exclude one electron from the field in which the photoelectron is moving. If the hole appeared in the state *i*, the corresponding frozen core HF equation for the new functions is

$$\left[-\frac{\nabla^2}{2}-\frac{Z_1}{r_1}-\frac{Z_2}{r_2}+\sum_{j\neq i}^{n}2J_{jj}(\boldsymbol{r})\right]\widetilde{\varphi}_{\varepsilon lm}(\boldsymbol{r})$$
$$-\sum_{j\neq i}^{n}J_{j,\widetilde{\varepsilon lm}}(\boldsymbol{r})\varphi_j(\boldsymbol{r})+J_{ii}(\boldsymbol{r})\widetilde{\varphi}_{\varepsilon lm}(\boldsymbol{r})+J_{i,\widetilde{\varepsilon lm}}(\boldsymbol{r})\varphi_i(\boldsymbol{r})$$
$$=\varepsilon\widetilde{\varphi}_{\varepsilon lm}(\boldsymbol{r})-\sum_{j=1}^{n}\varepsilon_{ij}\varphi_j(\boldsymbol{r}), \tag{21}$$

where the off-diagonal energy multipliers ε_{ij} are determined by the relation

$$\varepsilon_{ij}=\langle i,\widetilde{\varepsilon lm}|U|j,i\rangle. \tag{22}$$

The new excited state wave functions $\widetilde{\varphi}_{\varepsilon lm}(\boldsymbol{r})$ are connected with the wave functions found in the field of a neutral molecule $\varphi_{\varepsilon lm}(\boldsymbol{r})$ by the equation

$$\langle\widetilde{\varepsilon lm}|=\langle\varepsilon lm|+\sum_{\varepsilon'>F}\sum_{l'}\frac{\langle\varepsilon' l' m|}{\omega-\varepsilon'+\varepsilon_i+i\delta}\langle i,\widetilde{\varepsilon lm}|U|\varepsilon' l' m,i\rangle. \tag{23}$$

To check it, one should act on Eq. (23) by the operator $H_{\mathrm{HF}}-\varepsilon$, where H_{HF} means the operator in the right-hand side of Eq. (19) for which $\varphi_{\varepsilon lm}(\boldsymbol{r})$ are the eigenfunctions. As a result Eq. (21) is obtained.

From Eq. (23) it immediately follows that the dipole matrix element calculated with the new excited state wave function satisfies the following equation:

$$\langle\widetilde{\varepsilon lm}|d_\mu|i\rangle=\langle\varepsilon lm|d_\mu|i\rangle+\sum_{\varepsilon'>F}\sum_{l'}\frac{\langle\varepsilon' l' m|d_\mu|i\rangle}{\omega-\varepsilon'+\varepsilon_i+i\delta}\langle i,\widetilde{\varepsilon lm}|U|\varepsilon' l' m,i\rangle \tag{24}$$

It is easy to check that this equation takes into account the terms with $i=j$ of the RPA equation (16). Just these terms contain the divergent Coulomb matrix element $\langle i,\varepsilon lm|V|i,\varepsilon lm\rangle$, therefore the redefinition of the excited state wave functions allows to avoid the problem of divergent matrix elements [8]. The terms taken into account by Eq. (24) should be omitted when solving the RPA equation with the dipole and Coulomb matrix elements calculated with the redefined wave functions. So, if the ground state HF wave functions are determined by Eq. (19) and the excited state wave functions are determined by Eqs. (21) and (22), the RPA equation (16) for the projections of the dipole moment takes the form

$$\langle\varepsilon l(m_i+\mu)|D_\mu|i\rangle=\langle\varepsilon l(m_i+\mu)|d_\mu|i\rangle+\sum_{\substack{j\leqslant F\\(j\neq i)}}\sum_{\varepsilon'>F}\sum_{l'}\frac{\langle\varepsilon' l'(m_j+\mu)|D_\mu|j\rangle\langle j,\varepsilon l(m_i+\mu)|U|\varepsilon' l'(m_j+\mu),i\rangle}{\omega-\varepsilon'+\varepsilon_j+i\delta}$$
$$-\sum_{j\leqslant F}\sum_{\varepsilon'>F}\sum_{l'}\frac{\langle j|D_\mu|\varepsilon' l'(m_j+\mu)\rangle\langle\varepsilon' l'(m_j-\mu),\varepsilon l(m_i+\mu)|U|j,i\rangle}{\omega+\varepsilon'-\varepsilon_j-i\delta}, \tag{25}$$

where the selection rules for the projection of the orbital angular momentum m were taken into account explicitly. To solve this integral equation numerically, we replace the infinite upper limit of integration by a finite one, which can be done since the integrand decreases fast enough, and the integration over energy ε is replaced by integration over momentum k in order to integrate more accurately the region near the ionization threshold where the cross section is varying rather fast. Then the definite integral in finite limits is approximately replaced by a sum. This procedure enables one to transform the linear integral equation (25) into a system of linear algebraic equations which is solved by inversion of a matrix as it has been described in more details in [8]. Equation (25) contains a pole, therefore the integral in it can be written as

$$\int\frac{\langle\varepsilon' l'(m_j+\mu)|D_\mu|j\rangle\langle j,\varepsilon l(m_i+\mu)|U|\varepsilon' l'(m_j+\mu),i\rangle}{\omega-\varepsilon'+\varepsilon_j+i\delta}d\varepsilon'$$
$$=\mathrm{Pr}\int\frac{\langle\varepsilon' l'(m_j+\mu)|D_\mu|j\rangle\langle j,\varepsilon l(m_i+\mu)|U|\varepsilon' l'(m_j+\mu),i\rangle}{\omega-\varepsilon'+\varepsilon_j}d\varepsilon'+i\pi r, \tag{26}$$

where the integral in the right hand side should be understood in the principal value sense, and r is the residue in the pole

$$r=\langle\varepsilon' l'(m_j+\mu)|D_\mu|j\rangle\langle j,\varepsilon l(m_i+\mu)|U|\varepsilon' l'(m_j+\mu),i\rangle|_{\varepsilon'=\omega+\varepsilon_j}. \tag{27}$$

Due to that the solution is a complex value, and it can be written symbolically as

$$D_\mu=\mathrm{Re}\,D_\mu+i\,\mathrm{Im}\,D_\mu. \tag{28}$$

After inserting Eqs. (26)–(28) into Eq. (25) the solution of the RPA equation can be written in the matrix form as

$$(\mathrm{Re}\,D_\mu, \mathrm{Re}\,\tilde{D}_\mu, \mathrm{Im}\,D_\mu, \mathrm{Im}\,\tilde{D}_\mu) = (d_\mu, \tilde{d}_\mu, 0, 0)\cdot G^{-1}. \tag{29}$$

Here $D_\mu = \langle \varepsilon l(m_i+\mu)|D_\mu|i\rangle$, $\tilde{D}_\mu = \langle i|D_\mu^*|\varepsilon l(m_i+\mu)\rangle$, the row vectors have the dimension $4N$, and the square matrix G has the dimension $4N\times 4N$, with N being the total number of the excited states of discrete and continuous spectra calculated in all channels. The RPA matrix G has the following structure:

$$G = \begin{pmatrix} 1 & 0 \\ 0 & 1 \end{pmatrix} - \begin{pmatrix} A & B \\ -B & A \end{pmatrix}, \tag{30}$$

where the submatrices A and B have the dimensions $2N\times 2N$,

$$A = \begin{pmatrix} \left.\dfrac{\sqrt{2\varepsilon'}\langle \varepsilon l(m_i+\mu); j|U|i; \varepsilon' l'(m_j+\mu)\rangle}{\omega-\varepsilon'+\varepsilon_j}\right|_{j\neq i} & \dfrac{\sqrt{2\varepsilon'}\langle \varepsilon l(m_i+\mu); \varepsilon' l'(m_j-\mu)|U|i,j\rangle}{\omega-\varepsilon'+\varepsilon_j} \\ \dfrac{\sqrt{2\varepsilon'}\langle \varepsilon l(m_i+\mu); \varepsilon' l'(m_j-\mu)|U|i,j\rangle}{-\omega-\varepsilon'+\varepsilon_j} & \left.\dfrac{\sqrt{2\varepsilon'}\langle \varepsilon l(m_i+\mu); j|U|i; \varepsilon' l'(m_j+\mu)\rangle}{-\omega-\varepsilon'+\varepsilon_j}\right|_{j\neq i} \end{pmatrix}, \tag{31}$$

and in the matrix B only the residues in the poles are contributing [see Eqs. (26) and (27)], that is only the lines corresponding to $\varepsilon' = \omega+\varepsilon_j$ are different from zero

$$B_{\varepsilon'} = \pi\langle \varepsilon l(m_i+\mu); j|U|i; \varepsilon' l'(m_j+\mu)\rangle, \quad \pi\langle \varepsilon l(m_i+\mu); \varepsilon' l'(m_j-\mu)|U|i,j\rangle|_{\varepsilon'=\omega+\varepsilon_j}. \tag{32}$$

The three-points Lagrange interpolation formula is used for approximating the residue value r, and the Simpson formula in numerical integration when transforming the integral RPA equation to the linear system, as it was described in more detail in [8].

We need to solve the RPA equation (25) separately for $\mu=0$ and $\mu=+1$ (or -1), and also separately for the dipole matrix elements in the length and velocity forms. The solutions are inserted into Eq. (5) to calculate the photoionization cross section.

C. The numerical procedure

The HF equations are solved in prolate spheroidal coordinates ξ, η, φ defined as usual

$$\xi = (r_1+r_2)/R, \quad \eta = (r_1-r_2)/R,$$
$$1\leqslant\xi\leqslant\infty, \quad -1\leqslant\eta\leqslant 1, \quad 0\leqslant\varphi\leqslant 2\pi, \tag{33}$$

where r_1 and r_2 are the distances to the nuclei, and R is the internuclear distance (equal to 2.068 a.u. in our calculations for N_2). Since previously the spheroidal coordinates were already used in calculations of the bound state wave functions [11,12], and we are using the same procedure for the bound states, it is worth while to mention only some features of the continuous spectrum wave function calculations. We are looking for the solutions of the HF equation (21) for $\varphi_{\varepsilon lm}(\boldsymbol{r})$ which correspond to a discrete set of the electron energy values $\varepsilon = k_i^2/2$, $i=1,2,\ldots N$, $k_i = k_0+(i-1)\Delta k$, where k_0 is usually equal to 0.1, Δk for different transitions is varied between 0.7 and 0.1, and N (which is always odd) between 21 and 37. That gives the set of points for the numerical integration in the RPA equation (25). For each ε_i we calculate L orthonormal continuum state wave functions in the form of partial wave expansion in spheroidal coordinates

$$\varphi_{\varepsilon lm}(\boldsymbol{r}) = \sum_{l'} X_{ll'}^{\varepsilon m}(\xi) Y_{l'm}(\eta,\varphi), \quad l = l_{\min,\ldots,} l_{\min}+2(L-1). \tag{34}$$

Usually $L=3$ was sufficient to achieve a good convergence. For homonuclear molecules like N_2 where the parity is a good quantum number, both l and l' in Eq. (34) are only even or only odd, and $l_{\min}=0$ or 1 for even or odd parity states, respectively. From the comparison between Eqs. (6) and (34) one can easily find the coefficients $c_{ll'}^{\varepsilon m}$ and phase shifts $\delta_{ll'}^{\varepsilon m}$ from the known asymptotic behavior of the corresponding functions $X_{ll'}^{\varepsilon m}(\xi)$.

The numerical integration of the HF equation over ξ is divided into two regions, $(1,\xi_0)$ and $(\xi_0,\xi_{\max})$ where $\xi_0-1 \ll 1$ and $\xi_{\max}=60$. In the first region the solution is presented in the form

$$X_{ll'}^{\varepsilon m}(\xi) = (\xi^2-1)^{\lambda/2}\sum_k a_{ll'}^{km}(\xi-1)^k. \tag{35}$$

In the second region the Numerov method is used for the numerical integration. In contrast with [10] the modified boundary conditions have been used here for the continuum wave function calculation

$$\sum_K (a_{ll'}^{km})^2 = 1, \quad X_{ll'}^{\varepsilon m}(\xi_{\max}) = 0,$$
$$l'\neq l, \quad l = l_{\min},\ldots,l_{\min}+2(L-1). \tag{36}$$

The first condition fixes the function on the molecular axis and improves convergency. It is achieved by the iterative process of determination of the phase $\delta_{ll'}^{\varepsilon m}$. The second condition gives the linear independency of the solutions with different l.

The nonlocal exchange interaction is fully taken into account in the procedure of the iterative numerical solution of the HF equation. This is done as usual by calculating the exchange potential at each iteration with the wave function obtained from the previous iteration [11,12].

III. RESULTS OF CALCULATIONS

The partial photoionization cross sections have been calculated for all four valence orbitals of N_2 molecule, namely for $3\sigma_g$, $1\pi_u$, $2\sigma_u$, and $2\sigma_g$. Correspondingly in the RPA equations (25) and (29) the many-electron correlations between all four shells have been taken into account. In the expansion (34) usually three terms were included. It was checked that the higher order terms are giving a negligible contribution. The experimental thresholds have been used in calculations which differ from the theoretical ones by about 2 eV (see Table I of [1]). Important is also that in the experiment the $3\sigma_g$ orbital is the outermost one, while in calculations the $1\pi_u$ orbital has the lowest ionization threshold. Due to this shift of ionization thresholds the cross sections in the length and velocity forms in the RPA do not coincide as they do when the theoretical thresholds are used. In order to keep the agreement between them, we multiplied the HF matrix elements in the length and velocity forms when solving Eq. (29) by the following correcting factor:

$$c=\sqrt{\frac{\omega+I_{\text{theor}}-I_{\text{expt}}}{\omega}}=\sqrt{\frac{\varepsilon+I_{\text{theor}}}{\varepsilon+I_{\text{expt}}}} \tag{37}$$

according to the equations

$$(d^L)_{\text{corr}}=c\,d^L, \quad (d^v)_{\text{corr}}=d^v/c, \tag{38}$$

where ω is the photon energy, ε is the photoelectron energy, I_{theor} and I_{expt} are the theoretical and the experimental ionization thresholds of the shell (positive values), respectively. This correction allows us to greatly reduce the difference between the length and velocity cross sections in RPA appearing when the experimental thresholds are used.

Let us consider now the partial photoionization cross sections for each shell separately. Figure 1 shows our results for the outermost $3\sigma_g$ orbital. In the HF approximation the cross sections in the length and velocity forms usually differ by 20–30 %, while in the RPA they nearly coincide, therefore only one RPA curve is shown in the most cases below. Our HF cross sections for the $3\sigma_g \rightarrow \varepsilon\sigma_u$ transition are in a close agreement with the results of [2,5] both in the length and velocity forms, as well as with the length results reported in [7,21–23]. The broad σ^* shape resonance near 30 eV is reproduced fairly well already in the HF approximation, and does not appear to be sensitive to the details of numerical calculations. The inclusion of the RPA correlations increases the cross section for this transition at all photon energies, and

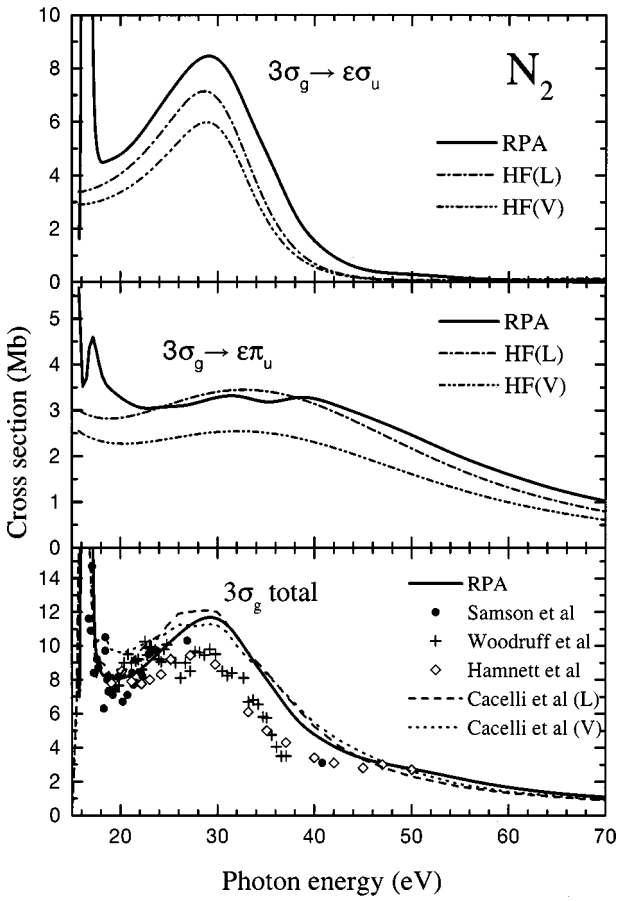

FIG. 1. Partial photoionization cross sections for different transitions from the $3\sigma_g$ orbital of N_2 molecule in the HF and RPA approximations calculated in the length (L) and velocity (V) forms. In the RPA the L and V cross sections nearly coincide, therefore only one line is shown. The experimental data are taken from Samson *et al.* [24], Woodruff and Marr [25], and Hamnett *et al.* [26]. The theoretical results of Cacelli *et al.* [1] in RPA are also shown.

just above the threshold a sharp peak appears corresponding to the strong $1\pi_u \rightarrow 1\pi_g$ resonance excitation. Figure 2 shows the influence of different two-channel correlations on the partial $3\sigma_g \rightarrow \varepsilon\sigma_u$ cross section. Evidently, the largest effect is given by the correlations with the $1\pi_u \rightarrow \varepsilon\pi_g$ transition.

The cross section for the $3\sigma_g \rightarrow \varepsilon\pi_u$ transition in the HF approximation is rather flat in a broad energy range, and our length result is in agreement with that of [22,23]. The influence of correlations on the $3\sigma_g \rightarrow \varepsilon\pi_u$ transition is less pronounced. Finally, the total photoionization cross section for the production of $N_2^+(X^2\Sigma_g{}^+)$ state in the RPA is shown in the lower part of Fig. 1. The maximum in the shape resonance is higher in magnitude and shifted to higher energies as compared to the experimental data, so that the HF result is even in a better agreement with the experiment than the RPA one. The analogous results in the RPA have also been obtained by the other authors [1,4,5], and for comparison the results of [1] are shown in the figure.

Figure 3 shows our cross sections calculated for the $1\pi_u$ orbital. In the HF approximation our cross sections for the

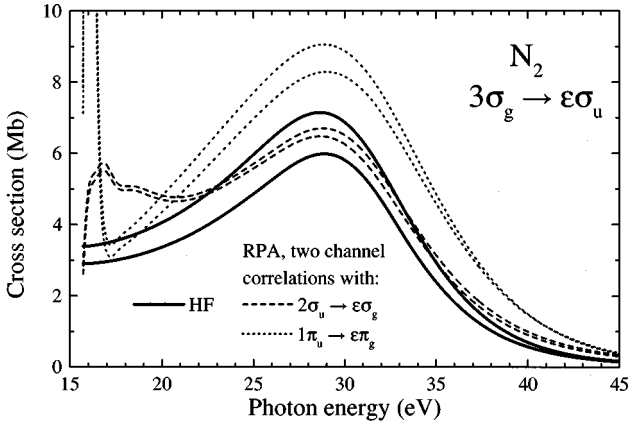

FIG. 2. Comparison between the cross sections for the $3\sigma_g \rightarrow \varepsilon\sigma_u$ transition calculated in the HF approximation and in the RPA taking into account different two-channel correlations separately. In all cases the upper line corresponds to the cross section in the length form and the lower one in the velocity form.

transitions $1\pi_u \rightarrow \varepsilon\sigma_g$ and $1\pi_u \rightarrow \varepsilon\delta_g$ are in a good agreement with the analogous results of [27]. As to the $1\pi_u \rightarrow \varepsilon\pi_g$ transition, it usually has an unphysical behavior in the HF approximation, namely, a very strong maximum just above the ionization threshold mentioned in several earlier publications [7,21,27]. We are using another method to perform calculations for this transition. Namely, we are solving Eq. (22) for the $\varepsilon\pi_g$ HF wave functions which does not contain the terms given by Eqs. (57) and (58) of [21], that is the terms corresponding to the interaction between the transitions $1\pi_u^+ \rightarrow \varepsilon\pi_g^+$ and $1\pi_u^- \rightarrow \varepsilon\pi_g^-$ where the superscript + or − means the sign of projection *m*. These terms are taken into account later when solving the RPA equation (25). As a result, in the HF approximation we do not have the strong maximum in the continuum, but we do have it when the one channel correlations between the $1\pi_u^+ \rightarrow \varepsilon\pi_g^+$ and $1\pi_u^- \rightarrow \varepsilon\pi_g^-$ transitions only are taken into account, as is shown in Fig. 4, in accord with the previous conclusions (we call these correlations as one channel correlations since the bound states $1\pi_u^+$ and $1\pi_u^-$ are degenerate and are described by the same wave functions). Nevertheless the maximum in our case is not as strong as in [7,21,27] because in Eq. (25) we are taking into account both time forward and time backward terms simultaneously while in the HF equation only the time forward terms are included. It is worth while to mention that the time forward terms are giving much larger contribution than the time backward terms, and that the diagonal time forward terms are contributing only in the case of 1π shell ionization due to our particular choice of the initial HF wave functions. In the case of ionization of $n\sigma$ shells the diagonal time forward terms are fully taken into account by the HF wave functions as it was described above [see Eq. (24)], and therefore the inclusion of the RPA correlations within one channel means the inclusion of time backward terms only which have a minor effect on the cross section, mainly bringing the length and velocity cross sections closer to each other. The influence of correlations with the other shells on the $1\pi_u \rightarrow \varepsilon\pi_g$ transition is also shown in Fig. 4. Since in all two channel calculations shown in Fig. 4 the RPA correlations between the $1\pi_u^+ \rightarrow \varepsilon\pi_g^+$ and $1\pi_u^- \rightarrow \varepsilon\pi_g^-$ transitions discussed above are always

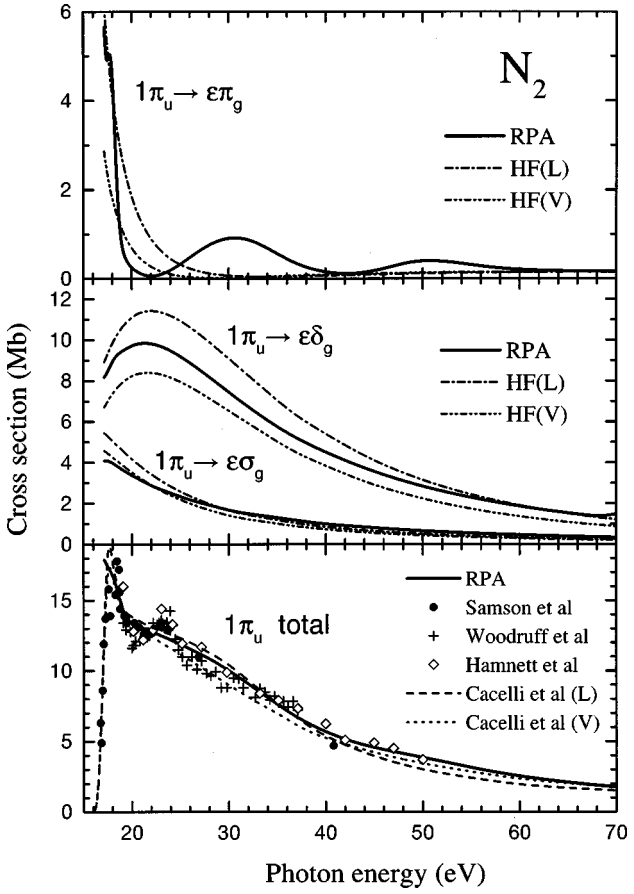

FIG. 3. The same as in Fig. 1 for the $1\pi_u$ orbital of N_2 molecule.

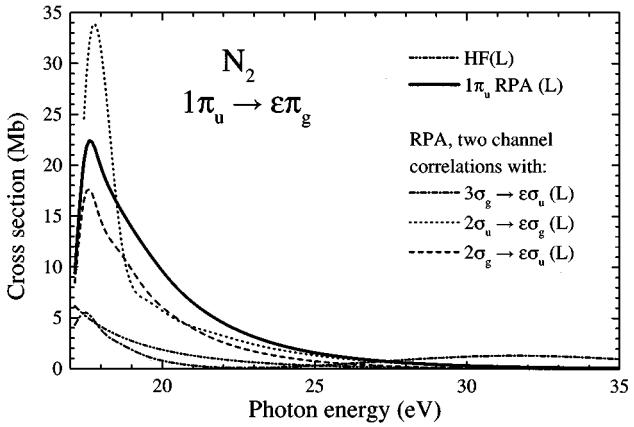

FIG. 4. Comparison between different cross sections for the $1\pi_u \rightarrow \varepsilon\pi_g$ transition. For simplicity, only the length form results are shown; in the velocity form the cross sections are 10–50 % lower. Thin full line shows the HF cross section from Fig. 3; thick full line is the RPA result with one-channel correlations between the $1\pi_u^+ \rightarrow \varepsilon\pi_g^+$ and $1\pi_u^- \rightarrow \varepsilon\pi_g^-$ transitions only taken into account (see text for details). The RPA results with different two-channel correlations taken into account separately are shown as explained in the figure.

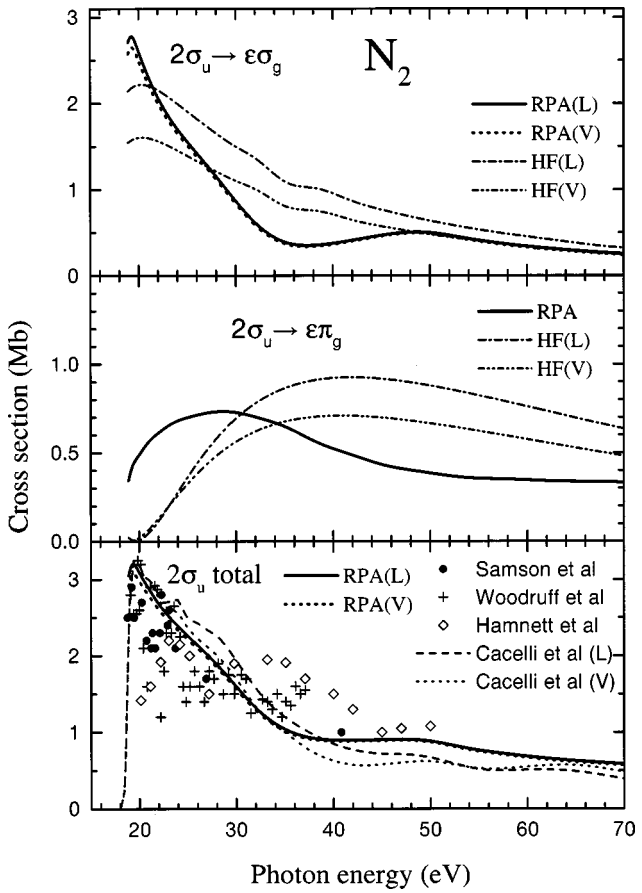

FIG. 5. The same as in Fig. 1 for the $2\sigma_u$ orbital of N_2 molecule.

taken into account, and since these correlations are very strong, it is more appropriate to compare the results of two channel calculations not with the HF cross section (as we do in all other cases) but with the RPA one channel cross section shown in Fig. 4 by full line. In particular, the interaction with the $2\sigma_u \rightarrow \varepsilon\sigma_g$ transition increases further the cross section near threshold but makes it smaller at higher energies, while the $3\sigma_g \rightarrow \varepsilon\sigma_u$ transition greatly reduces the cross section in the vicinity of threshold and creates a small second maximum at about 32 eV. The interaction with the $2\sigma_g \rightarrow \varepsilon\sigma_u$ transition reduces the cross section below 30 eV and produces a small additional maximum at about 50 eV. These interactions explain the complicated behavior of the fully correlated cross section for the $1\pi_u \rightarrow \varepsilon\pi_g$ transition in RPA shown in Fig. 3.

The total cross section for the production of $N_2^+(A^2\Pi_u)$ state is presented in the lower part of Fig. 3. In general, there is a good agreement with the experimental data, as well as with the RPA results of [1] and [4]. We could not reproduce the maximum at 23 eV which is connected with the simultaneous excitation of one $3\sigma_g$ and one $1\pi_u$ electrons into the discrete excited states with the subsequent autoionization decay [28–30] because the two-electron processes are not taken into account by the RPA method.

Figure 5 shows the results for the $2\sigma_u$ shell. In the HF approximation the agreement with the previous calculations

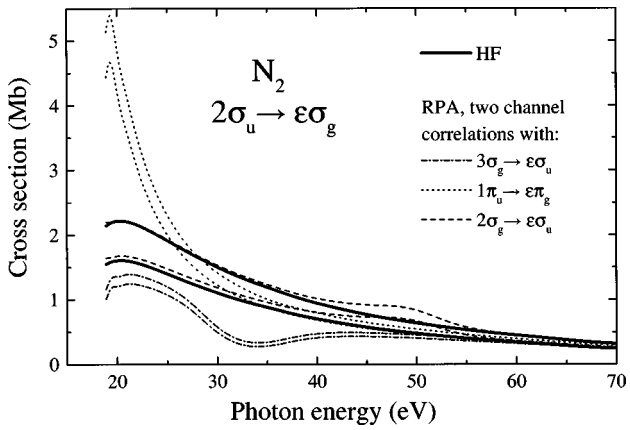

FIG. 6. The same as in Fig. 2 for the $2\sigma_u \rightarrow \varepsilon\sigma_g$ transition.

is not as good as before. For the $2\sigma_u \rightarrow \varepsilon\sigma_g$ transition our cross section has a maximum 1 eV above threshold, while the cross sections published in [7,22] have the maximum at about 10 eV above threshold, though the magnitudes of the cross sections are similar. The cross section for the $2\sigma_u \rightarrow \varepsilon\pi_g$ transition published in [22] has some additional maximum at about 33 eV photon energy which is absent in our case. It was mentioned by several authors that the interchannel interaction is particularly important for this shell [31,1,4]. Figure 6 demonstrates the strong influence of different two-channel interactions on the cross section of the $2\sigma_u \rightarrow \varepsilon\sigma_g$ transition. From these curves it is evident that the maximum at the threshold (see Fig. 5) is mainly due to the interaction with the $1\pi_u \rightarrow \varepsilon\pi_g$ channel, the minimum at about 37 eV appears due to the influence of the $3\sigma_g \rightarrow \varepsilon\sigma_u$ channel, and the second maximum at about 50 eV is the result of the interactions with both $3\sigma_g \rightarrow \varepsilon\sigma_u$ and $2\sigma_g \rightarrow \varepsilon\sigma_u$ channels. Figure 7 shows the analogous results for the $2\sigma_u \rightarrow \varepsilon\pi_g$ transition. Here the important role play only the correlations with the $3\sigma_g \rightarrow \varepsilon\pi_u$ channel which reduce the cross section by approximately a factor of 2 and brings the length and velocity cross sections much closer to each other. The influence of correlations with the $1\pi_u \rightarrow \varepsilon\sigma_g$ channel is rather small and is not shown in Fig. 7. The fully correlated cross section for the $2\sigma_u \rightarrow \varepsilon\pi_g$ transition shown in Fig. 5 essentially follows the behavior of the cross section

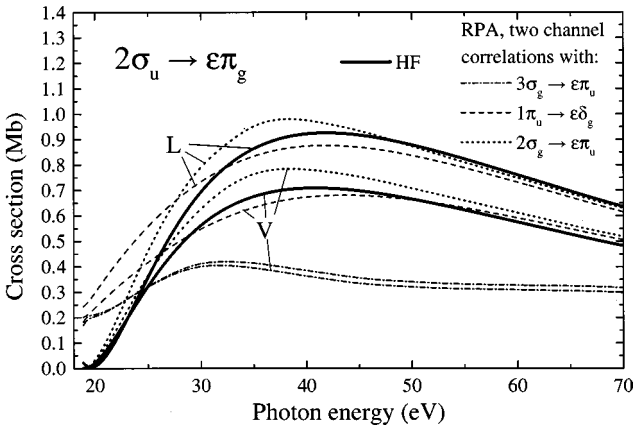

FIG. 7. The same as in Fig. 2 for the $2\sigma_u \rightarrow \varepsilon\pi_g$ transition.

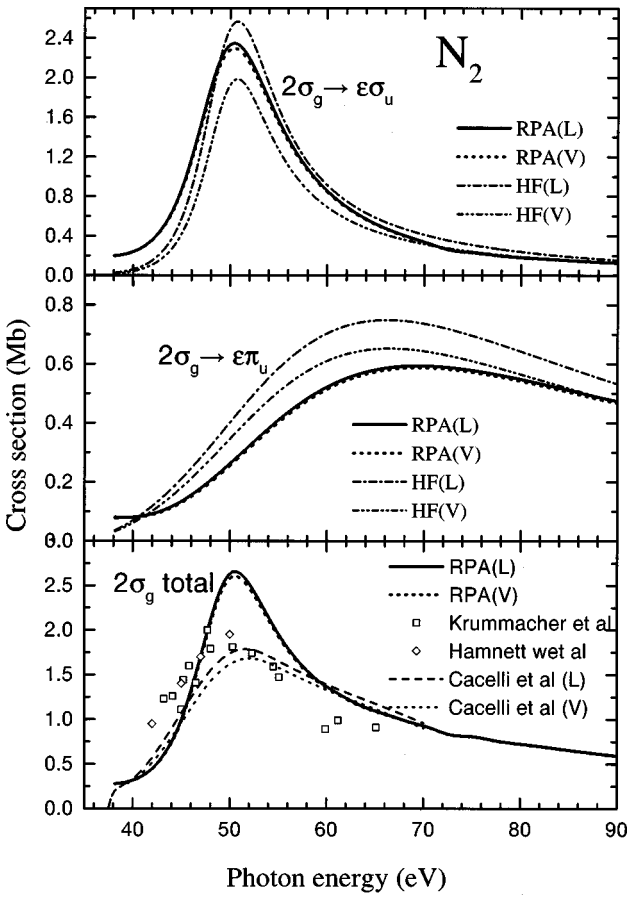

FIG. 8. The same as in Fig. 1 for the $2\sigma_g$ orbital of N_2 molecule. The experimental data are from Krummacher *et al.* [32] and Hamnett *et al.* [26].

corresponding to the two channel interaction with the $3\sigma_g \rightarrow \varepsilon\pi_u$ channel.

The total cross section for the production of $N_2^+(B^2\Sigma_u^+)$ state shown in the lower part of Fig. 5 is in a good agreement with the RPA results of [1] and [4]. The experimental data for this shell are rather unsteady, therefore it is difficult to judge whether the agreement of the RPA result with the experiment is good or not, but it is likely that at photon energies between 30 and 45 eV our RPA cross section is too small.

The cross sections for ionization of the $2\sigma_g$ shell are presented in Fig. 8. In the HF approximation our cross section for the $2\sigma_g \rightarrow \varepsilon\sigma_u$ channel in the shape resonance is a factor of 1.6 higher than in the previous calculations [7]. The role of correlations for this shell is less pronounced, partly because its ionization threshold is about 20 eV higher than the ionization thresholds of three other valence shells. The total photoionization cross section in the RPA in the maximum of the shape resonance is about 30% higher than both the experimental cross section and the RPA cross section of Cacelli *et al.* [1]. The deviation from the experiment can be attributed to the influence of the vibrational motion [33], and probably also to core relaxation [34] which for the innermost valence shell can play some role.

Figure 9 shows the total photoionization cross section calculated in the RPA and compared with the experimental data. Since our length and velocity cross sections nearly coincide, only one RPA result is shown in the figure. There is a good overall agreement with the experiment, though in the photon energy region between 18 and 38 eV the experimental points are somewhat lower than our curve. We also could not reproduce the sharp variation of the experimental cross section around 23 eV which is connected with the simultaneous excitation of one $3\sigma_g$ and one $1\pi_u$ electrons into the discrete excited states with the subsequent autoionization decay [28–30]. These two-electron excitation processes are not taken into account in the RPA method. In general, our cross section is rather close to the recent RPA results of Cacelli *et al.* [1] obtained in the same approximation, though in their calculations some difference between the length and velocity results remains.

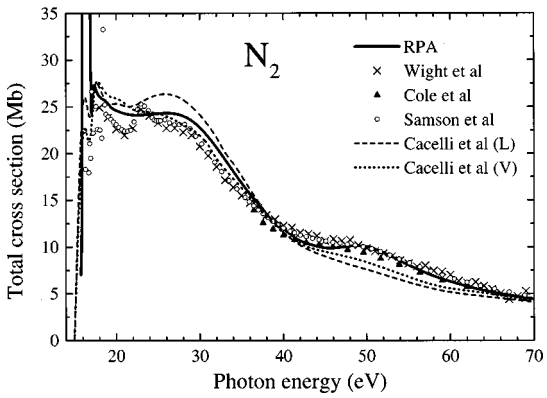

FIG. 9. The total photoionization cross section of N_2 molecule calculated in the RPA approximation, the length and velocity results coincide within the thickness of the curve; therefore only one curve is shown. The theoretical results of Cacelli *et al.* [1] in RPA in the length (L) and velocity (V) forms are also shown. The experimental data are from Wight *et al.* [35], Cole and Dexter [36], and Samson *et al.* [37].

IV. CONCLUSIONS

The RPA method in the form developed earlier for atoms [8], is generalized here for diatomic molecules. The calculations of the Hartree-Fock wave functions of the discrete and continuous spectrum forming an orthonormal zero-order basis set have been performed in prolate spheroidal coordinates. In a numerical solution of the HF equations, the angular variables were separated by using the expansion of wave functions in spherical harmonics. The procedure of solving the RPA equations was similar to that used earlier in atomic calculations. The photoionization cross section of N_2 molecules calculated by this method in the photon energy range from ionization threshold up to 70 eV is in a good agreement with the recent experimental data. The partial photoionization cross sections for each shell separately have been also calculated and compared with the existing experimental data. The agreement between theory and experiment for the $3\sigma_g$ and $2\sigma_g$ shells is less satisfactory than for the $2\sigma_u$ and $1\pi_u$ shells, namely, the theoretical cross sections in the shape

resonances are too high. This discrepancy can be attributed to several effects not taken into account in our method. In particular, we used the fixed nuclei approximation, while it is known that the cross section, especially in the shape resonances, depends on the internuclear distance [33,23]. Therefore inclusion of the vibrational degree of freedom into consideration can modify our cross section. Another effect which we ignored is the core relaxation [34], which we believe can play some role in the calculations for the $2\sigma_g$ shell.

Since previously many calculations have been performed on the HF level, it was demonstrated explicitly what is the influence of different intershell RPA correlations on the HF cross section. The results show that unlike the atomic nitrogen [38], the many-electron correlations in the molecular nitrogen are very important. This is because the correlations between closely spaced many electron shells are usually the most important, and in N_2 there are eight electrons in three closely spaced valence shells, $3\sigma_g$, $1\pi_u$, and $2\sigma_u$, having the ionization potentials within just a few eV. The present work together with our recent investigation of the photoionization of H_2 molecule [10] demonstrate a high reliability of the RPA method developed by us for molecular photoionization cross section calculations.

ACKNOWLEDGMENTS

The authors thank Professor V. McKoy and Dr. G. Raseev for fruitful discussions. This research was supported by a joint grant of the Deutsche Forschungsgemeinschaft (Grant No. 436 RUS 113/372) and the Russian Fund for Basic Research (Grant No. 96-02-00155G). S.K.S. and N.A.C. are grateful for the hospitality of the Johannes-Gutenberg Universität Mainz extended to them during the work on this paper. N.A.C. also gratefully acknowledges the financial support of the Ministry of Education, Science and Culture of Japan and the hospitality of the Photon Factory extended to him at the final stage of the work on this paper.

[1] I. Cacelli, R. Moccia, and A. Rizzo, Phys. Rev. A **57**, 1895 (1998).
[2] J. Schirmer and F. Mertins, J. Phys. B **29**, 3559 (1996).
[3] L. Veseth, J. Phys. B **27**, 481 (1994).
[4] R. R. Lucchese and R. W. Zurales, Phys. Rev. A **44**, 291 (1991).
[5] S. Yabushita, C. W. McCurdy, and T. N. Rescigno, Phys. Rev. A **36**, 3146 (1987).
[6] P. Swanstrom, J. T. Golab, D. L. Yeager, and J. A. Nichols, Chem. Phys. **110**, 339 (1986).
[7] G. R. J. Williams and P. W. Langhoff, Chem. Phys. Lett. **78**, 21 (1981).
[8] M. Ya. Amusia and N. A. Cherepkov, Case Stud. At. Phys. **5**, 47 (1975).
[9] M. Ya. Amusia, in *VUV and Soft X-Ray Photoionization Studies*, edited by U. Becker and D. A. Shirley (Plenum, New York, 1996), p. 1.
[10] S. K. Semenov and N. A. Cherepkov, Chem. Phys. Lett. **291**, 375 (1998).
[11] E. A. McCullough, Jr., J. Chem. Phys. **62**, 3991 (1977).
[12] L. Laaksonen, P. Pyykko, and D. Sundholm, Comput. Phys. Rep. **4**, 313 (1986).
[13] Q. Zheng, A. K. Edwards, R. M. Wood, and M. A. Mangan, Phys. Rev. A **52**, 3945 (1995).
[14] P. A. Christiansen and E. A. McCullough, Jr., J. Chem. Phys. **67**, 1877 (1977).
[15] D. Dill and J. L. Dehmer, J. Chem. Phys. **61**, 692 (1974).
[16] A. F. Starace, in *Handbuch der Physik*, edited by W. Mehlhorn (Springer-Verlag, Berlin, 1982), Vol. 31, p. 1.
[17] H. Park and R. N. Zare, J. Chem. Phys. **104**, 4554 (1996).
[18] D. I. Abramov and I. V. Komarov, Teor. Mat. Fiz. **22**, 253 (1975).
[19] D. Loomba, S. Wallace, and D. Dill, J. Chem. Phys. **75**, 4546 (1981).
[20] E. Shigemasa, J. Adachi, K. Soejima, N. Watanabe, A. Yagishita, and N. A. Cherepkov, Phys. Rev. Lett. **80**, 1622 (1998).
[21] R. R. Lucchese, G. Raseev, and V. McKoy, Phys. Rev. A **25**, 2572 (1982).
[22] T. N. Rescigno, C. F. Bender, B. V. McKoy, and P. W. Langhoff, J. Chem. Phys. **68**, 970 (1978).
[23] G. Raseev, H. Le Rouzo, and H. Lefebvre-Brion, J. Chem. Phys. **72**, 5701 (1980).
[24] J. A. R. Samson, G. N. Haddad, and J. L. Gardner, J. Phys. B **10**, 1749 (1977).
[25] P. R. Woodruff and G. V. Marr, Proc. R. Soc. London, Ser. A **358**, 87 (1977).
[26] A. Hamnett, W. Stoll, and C. E. Brion, J. Electron Spectrosc. Relat. Phenom. **8**, 367 (1976).
[27] T. N. Rescigno, A. Gerwer, B. V. McKoy, and P. W. Langhoff, Chem. Phys. Lett. **66**, 116 (1979).
[28] K. Codling, Astrophys. J. **143**, 552 (1966).
[29] P. Gurtler, V. Saile, and E. E. Koch, Chem. Phys. Lett. **48**, 245 (1977).
[30] R. E. Stratmann, G. Bandarage, and R. R. Lucchese, Phys. Rev. A **51**, 3756 (1995).
[31] J. A. Stephens and D. Dill, Phys. Rev. A **31**, 1968 (1985).
[32] S. Krummacher, V. Schmidt, and F. Wuilleumier, J. Phys. B **13**, 3993 (1980).
[33] J. L. Dehmer, D. Dill, and S. Wallace, Phys. Rev. Lett. **43**, 1005 (1979).
[34] D. L. Lynch and V. McKoy, Phys. Rev. A **30**, 1561 (1984).
[35] G. R. Wight, M. J. Van der Wiel, and C. E. Brion, J. Phys. B **9**, 675 (1976).
[36] B. E. Cole and R. N. Dexter, J. Phys. B **11**, 1011 (1978).
[37] J. A. R. Samson, T. Masuoka, P. N. Pareek, and G. C. Angel, J. Chem. Phys. **86**, 6128 (1987).
[38] N. A. Cherepkov, L. V. Chernysheva, V. Radojevic, and I. Pavlin, Can. J. Phys. **52**, 349 (1974).